Supplement of Hydrol. Earth Syst. Sci., 21, 2905–2922, 2017
https://doi.org/10.5194/hess-21-2905-2017-supplement
© Author(s) 2017. This work is distributed under
the Creative Commons Attribution 3.0 License.

Hydrology and Earth System Sciences
Open Access

Supplement of

Detecting seasonal and long-term vertical displacement in the North China Plain using GRACE and GPS

Linsong Wang et al.

Correspondence to: Linsong Wang (wanglinsong@cug.edu.cn)

The copyright of individual parts of the supplement might differ from the CC BY 3.0 License.

Section S1. The effects of non-tidal ocean and atmospheric variations loading on the GRACE model and GPS coordinates

The cause of the difference between our results and Liu's work (Liu et al., 2014) is that we removed atmospheric and non-tidal ocean loading effects but they did not. The atmospheric and non-tidal ocean were not considered in Liu's paper, in which they used the AOD1B (atmosphere and ocean de-aliasing level-1b) product to add back the de-aliasing atmospheric and non-tidal oceanic effects to the GRACE data, primarily because Liu et al. (2014) think these effects cannot be easily removed from the GPS height time series.

Taking into account the elastic deformation of the solid Earth under the variable load via the load Love number k_n for loading harmonic of degree n, we get the final formula:

$$C_{nm} = \frac{a^2(1+k_n)}{(2n+1)Mg} \iint\limits_{Earth} P_s\, P_{nm}(cos\theta) cos\lambda m dS$$

$$S_{nm} = \frac{a^2(1+k_n)}{(2n+1)Mg} \iint\limits_{Earth} P_s\, P_{nm}(cos\theta) sin\lambda m dS$$

The equation (3-7) from GRACE AOD1B Product Description Document (Flechtner, 2007).

Because in the current approach the de-aliasing ADO1B products are represented by a spherical harmonic series of degree and order 100 the following loading Love numbers are used (Dong et al, 1996; Farrell, 1972):

$$k_0 = 0; \quad k_1 = 0; \quad k_2 = -0.308; \quad k_3 = -0.195; \quad k_4 = -0.132$$

$$k_5 = -0.103; k_6 = -0.089; k_7 = -0.082; k_8 = -0.078; k_9 = -0.073$$

$$\text{for } k_{10} \text{ to } k_{17}: -\frac{0.682 + 0.27(n - 10)/8}{n}$$

$$\text{for } k_{18} \text{ to } k_{31}: -\frac{0.952 + 0.288(n - 18)/14}{n}$$

$$\text{for } k_{32} \text{ to } k_{55}: -\frac{1.24 + 0.612(n - 32)/24}{n}$$

$$\text{for } k_{56} \text{ to } k_{100}: -\frac{1.402 + 0.059(n - 56)/44}{n}$$

The load Love number k_n for loading harmonic of degree n, from GRACE AOD1B Product Description Document (Flechtner, 2007).

In our processing strategy, the AOD1B product was not added back to the GRACE Stokes coefficient, which means our GRACE-derived loading deformation did not include the atmospheric and non-tidal ocean effects. In order to remove the effects of atmospheric and non-tidal oceanic loading on the GPS coordinates, we computed the displacements due to atmospheric loading using data and programs developed by the GGFC (Global Geophysical Fluid Center) (T. van Dam, NCEP Derived 6 hourly, global surface displacements at 2.5°×2.5° degree spacing, http://geophy.uni.lu/ncep-loading.html, 2010), which utilized the NCEP (National Center of Environmental Protection) reanalysis surface pressure data set. The 12-hour sampling model, ECCO (Estimating the Circulation & Climate of the Ocean), is used to compute the surface displacement driven by non-tidal ocean effects and its spatial resolution is 1°× 0.3-1.0°. The loading effects of non-tidal ocean and atmospheric variations on the

GPS coordinates see the Figure S1.

In Liu's work, they added GRACE's Atmosphere and Ocean De-aliasing Level-1B (AOD1B) solution (GAC solution) to the GRACE spherical harmonic solutions. And they adopt the load Love numbers from Guo et al. (2004) to transform these coefficients into vertical surface deformation estimates. We check the two results of Love numbers (ocean-load and atmospheric pressure-load) from Guo et al. (2004), there are significant differences between ocean-load and atmospheric pressure-load Love numbers. Meanwhile, we compared k_n Love numbers from Guo et al. (2004) (Liu et al.'s work) and k_n Love numbers from Han and Wahr (1995) (our work) with the k_n Love numbers used in ADO1B products, respectively.

We found k_n from ocean-load Love numbers (Guo et al., 2004) and k_n Love numbers from Han and Wahr (1995) are not identical, but they look pretty close with the k_n Love numbers used in ADO1B products. However, k_n from atmospheric pressure-load Love numbers (Guo et al., 2004) shows a big difference with all other results (Figure S2). So, Liu et al. (2014) probably use the atmospheric pressure-load Love numbers to calculate the vertical displacements, and this approach leads to the fact that the amplitude of the same station from GRACE is much more than GPS and our GRACE results, which is caused by the significantly larger k_n from atmospheric pressure-load Love numbers (Guo et al., 2004) compared with Love numbers from Han and Wahr (1995) and Farrel (1972) (see the Table S2).

Figure S1(a) shows an example GPS site (BJFS) comparing the GRACE-modeled height displacements with (add GAD and GAA, shown as blue and red solid line, respectively) and without the AOD1B model (black solid line). Basing on GRACE solutions without the AOD1B model, the results also show the difference between the GRACE-modeled height displacements with not destriping (black dashed line) and after destriping (black solid line). In addition, after destriping and removing GLDAS/Noah model, GRACE-modeled (without the AOD1B model) height displacements show an obvious rising trend and the seasonal amplitudes are reduced (green solid line).

Figure S1(b) shows an example GPS site (BJFS) comparing GRACE AOD1B product with the loading effects of atmospheric and non-tidal ocean on the GPS coordinates from the NECP and ECCO data. It is clear that the loading effect of atmospheric (red solid line) and non-tidal ocean (blue solid line) from the AOD1B agrees with the NECP-modeled (black cross symbols) and (orange cross symbols) seasonal variations.

A comparison between seasonal amplitudes and phases fit of vertical displacements derived by GRACE and GPS for IGS stations after atmospheric and non-tidal ocean corrected and the non-corrected ones (Table S1). This is achieved by a simultaneous fit for the annual and semi-annual signals. GRACE-modeled amplitudes and phases of the vertical displacements due to seasonal loading show high correlation with GPS which observed seasonal position variations. This fact confirms that the hydrological and atmospheric mass cycle is the main cause of seasonal ground deformation in the NCP. When the effects of atmospheric and non-tidal ocean are removed, both GPS and GRACE show the seasonal hydrological variations, but amplitude and phase appear to have changes with varying degrees in GPS and GRACE. This result suggests that GPS measurements can sense the difference between loads very near the site, and loads a bit further away, but GRACE can not. Thus, the amplitude of GPS is basically greater than the GRACE data and the phase of different GPS sites shows obvious difference compared with GRACE. In other words, GRACE underestimates NCP vertical displacements at sites very near regions of concentrated loads, because GRACE solutions truncate to l_{max}=60, and so smooth out concentrated loads.

Section S2. Comparison between GPS and GRACE-derived seasonal variations

The vertical displacements are computed at the GPS sites from the GRACE-derived gravity field coefficients and compared with the GPS mesurements, and 24 selected stations (CMONOC) are shown in Figure S3. Besides, the horizontal seasonal (detrended and fit) displacements between GPS observed and GRACE-derived for site BJFS, BJSH, JIXN, TAIN and ZHNZ are shown in Figure S4. Although nearly half of the GPS data are missing 4~6 months from 2011 to 2012, we can also find that the seasonal variations of vertical surface displacement are in both GPS and GRACE solutions.

To quantitatively evaluate the consistency of seasonal variation between GPS and GRACE, the relative correlation coefficients of seasonal variation between GPS and GRACE are computed. We also remove GRACE-derived seasonal deformation from GPS observed detrended height time series, and compute the reductions of WRMS (Weighted Root-Mean-Squares) basing on the following equation (van Dam et al., 2007):

$$WRMS_{reduction}(\%) = \frac{WRMS_{GPS_i} - WRMS_{GPS_i - GRACE_i}}{WRMS_{GPS_i}} \times 100$$

Table S3 shows the correlation between GPS and GRACE derived seasonal variations and WRMS reduction ratio of removing GRACE-derived seasonal deformation from GPS observed detrended height time series (between non-corrected and after atmospheric and non-tidal ocean corrected).

Section S3. Long-term uplift due to the mass loss and GIA effects

Besides the significant seasonal variations discussed above, there is also a long-term uplift contained in GRACE-derived vertical displacement, which is primarily due to the TWS loss and potential GIA effects in the NCP.

Table S3 shows the seasonal amplitudes, phases and trend fit of vertical displacements between derived by GRACE and remove GLDAS-derived deformation from GRACE, the annual and semi-annual amplitude reduced nearly half after removing GLDAS-derived deformation from GRACE, but there is no obvious change for trend rate before and after removing GLDAS-derived deformation.

And GIA uplift rate for a compressible Earth was computed (results computed and provided by Geruo A) using the ICE5G ice history and VM2 viscosity profile (Peltier et al., 2004), which assumes a compressible Earth, and includes polar wander feedback, degree-one terms, and a self-consistent ocean. Figure S5 shows GIA effects from GPS measurements, which is about 0.2~0.4 mm/year in the land areas of China (a) and 0.28~0.33 mm/year in the NCP (b).

Section S4. Land subsidence in NCP

In order to verify vertical crust movement using the corrected vertical rates after subtracting the GRACE-derived long-term uplift rate due to load changes and GIA effects, we compare the previous study results from the vertical crust movement model between 2007~2013 (Figure S6a) (MLR, 2015) and the vertical motion in north China with high spatial resolution (Figure S6b) (Zhao et al., 2014). We find that our study agree with the previous study results which combining mobile and continuous GPS observation or leveling data. The results show that there are uplift areas and subsidence areas in NCP. Almost the whole central and eastern region of NCP suffers from serious ground subsidence, caused by the groundwater exploitation in the deep confined aquifers. In addition, in the most areas of Shanxi plateau shows ground uplifts lightly. The results reveal that the present vertical motion pattern of north China is consistent with neotectonic movement and human activities.

References

Dong, D., Fang, P., Bock, Y., Cheng, M. K., and Miyazaki, S.: Anatomy of apparent seasonal variations from GPS-derived site position time series, J. Geophys. Res., 107(B4), 2075, doi: 10.1029/2001JB000573, 2002.

Farrell, W. E.: Deformation of the Earth by surface loads, Rev. Geophys. Space Phys., 10, 761–797, doi: 10.1029/RG010i003p00761, 1972.

Flechtner, F.: GRACE AOD1B product description document for product releases 01 to 04, Tech. Rep., Rev. 3.1, GRACE Doc., 327–750, GeoForschungsZentrum Potsdam, Potsdam, Germany, 2007.

Guo, J. Y., Li, Y. B., Huang, Y., Deng, H. T., Xu, S. Q., and Ning, J. S.: Green's Function of Earth's Deformation as a Result of Atmospheric Loading, Geophys. J. Int., 159, 53–68, doi: 10.1111/j.1365-246X.2004.02410.x, 2004.

Han, D., and Wahr, J.: The viscoelastic relaxation of a realistically stratified Earth, and a further analysis of post-glacial rebound, Geophys. J. Int., 120, 287–311, 1995.

Liu, R. L., Li, J. C., Fok, H. S., Shum, C. K., and Li, Z.: Earth surface deformation in the North China Plain detected by joint analysis of GRACE and GPS data, Sensors, 14, 19861-19876, doi: 10.3390/s141019861, 2014.

Ministry of Land and Resources of China (MLR): Monitoring results of important geographical conditions in the Beijing-Tianjin-Hebei region, Ministry of Land and Res. of China, Beijing, http://www.mlr.gov.cn/, 2015.

Peltier, W. R.: Global glacial isostasy and the surface of the ice-age earth: The ice-5G (VM2) model and GRACE, Annu. Rev. Earth Planet. Sci., 32, 111-149, 2004.

van Dam, T., Wahr, J., and Lavallée, D.: A comparison of annual vertical crustal displacements from

GPS and Gravity Recovery and Climate Experiment (GRACE) over Europe, J. Geophys. Res., 112, B03404, doi: 10.1029/2006JB004335, 2007.

Zhao, B., Nie, Z. S., Huang, Y., Wang, W., Zhang, C. H., Tan, K., and Du, R. L.: Vertical motion of north China inferred from dense GPS measurements, J. Geodesy Geodyn., 34 (5), 35–39, 2014. (in Chinese with English abstract)

Figure S1. The effects of non-tidal ocean variations and atmospheric loading on the GRACE model and GPS coordinates.

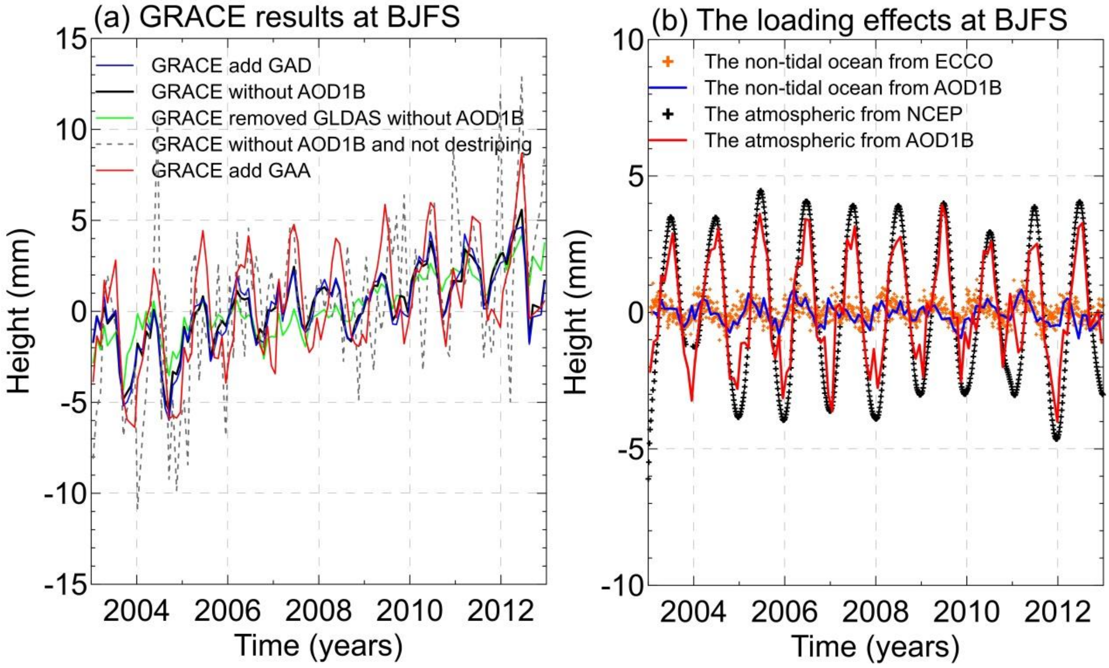

Figure S2. Compare with different k_n Love numbers.

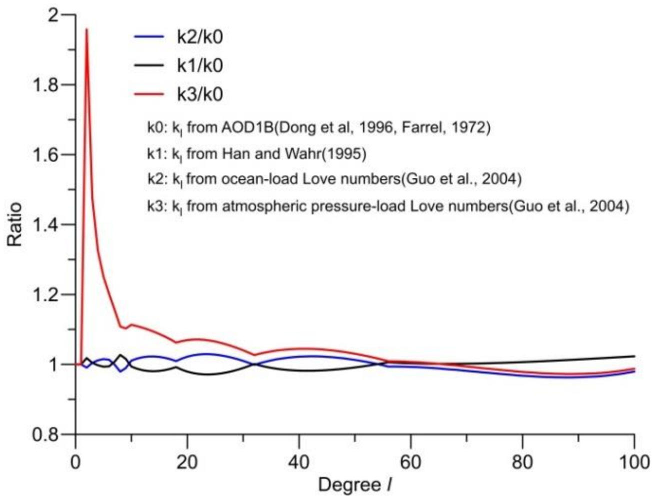

Figure S3. Comparison between GPS and GRACE-derived seasonal height variations at 24 GPS sites from CMONOC.

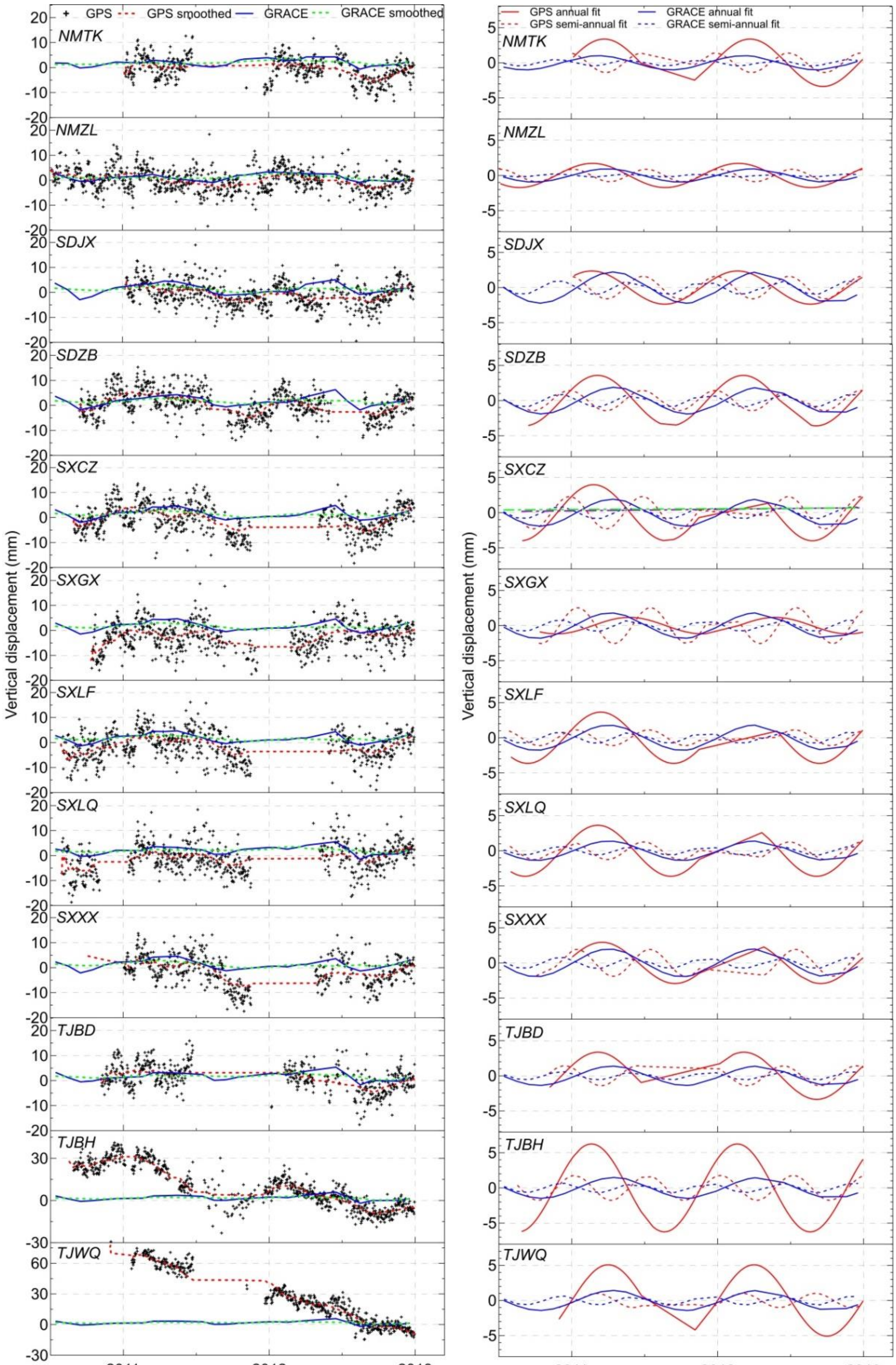

to be continued

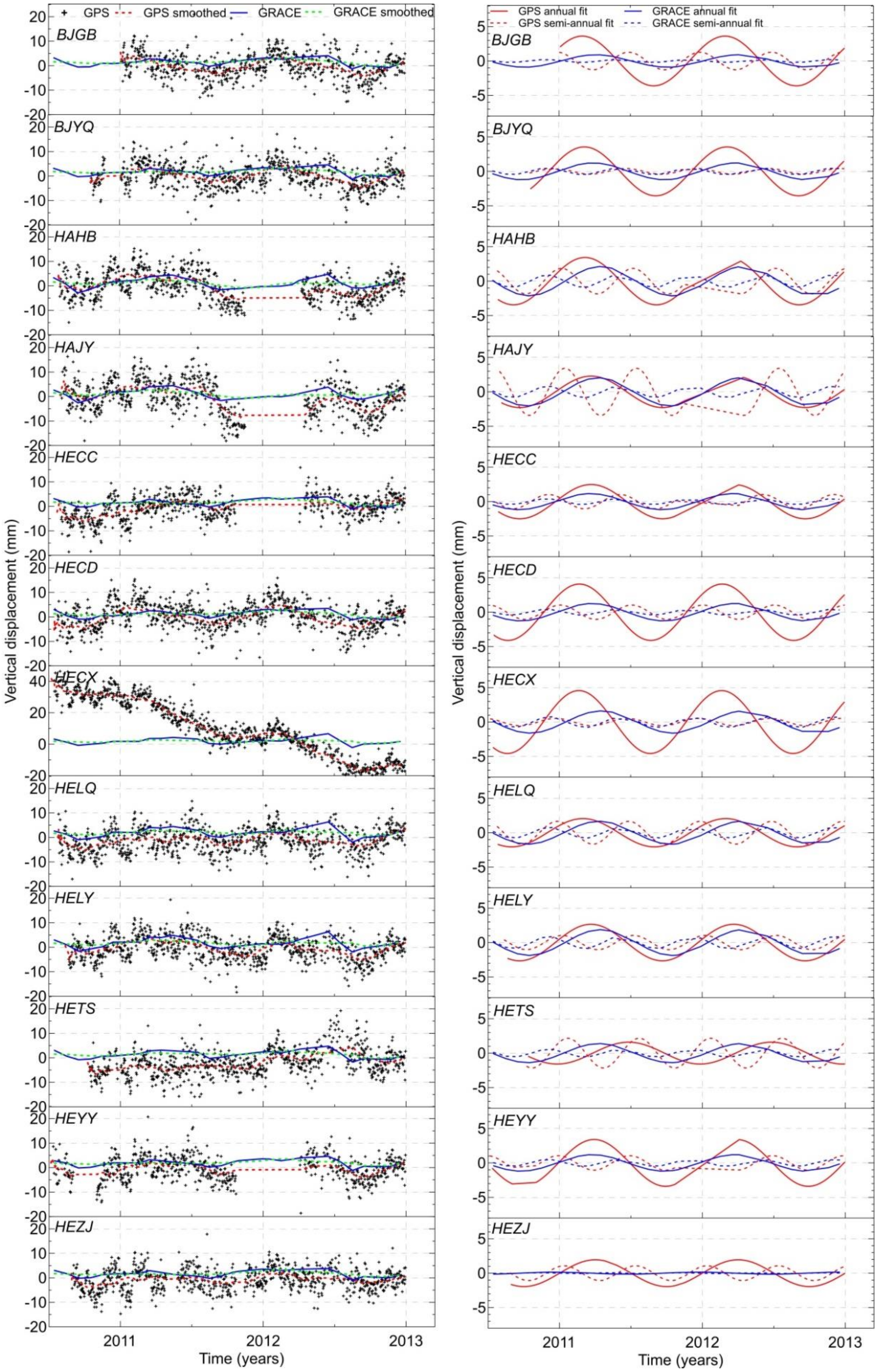
GPS
GPS smoothed
GRACE
GRACE smoothed
GPS annual fit
GPS semi-annual fit
GRACE annual fit
GRACE semi-annual fit
BJGB
BJYQ
HAHB
HAJY
HECC
HECD
HECX
HELQ
HELY
HETS
HEYY
HEZJ
Vertical displacement (mm)
Time (years)
2011
2012
2013

Figure S4. Comparison between GPS observed and GRACE-derived horizontal seasonal (detrended and fit) displacements for site BJFS, BJSH, JIXN, TAIN and ZHNZ.

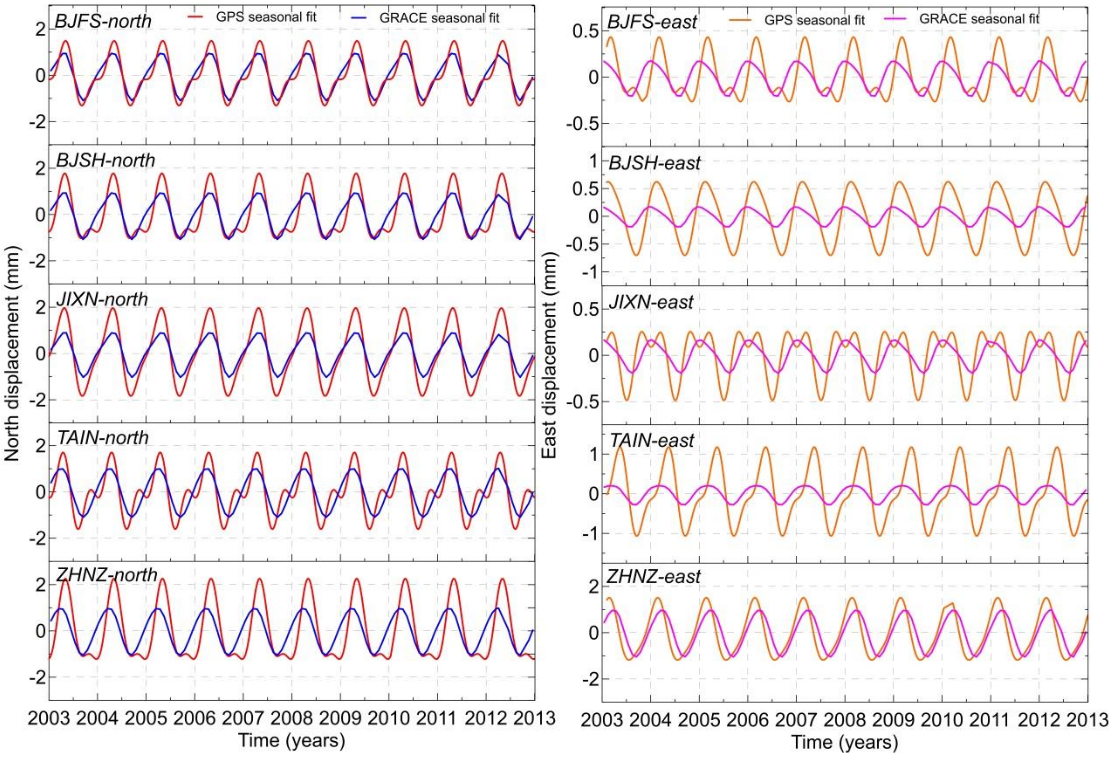

Figure S5. Long-term uplift due to GIA effects

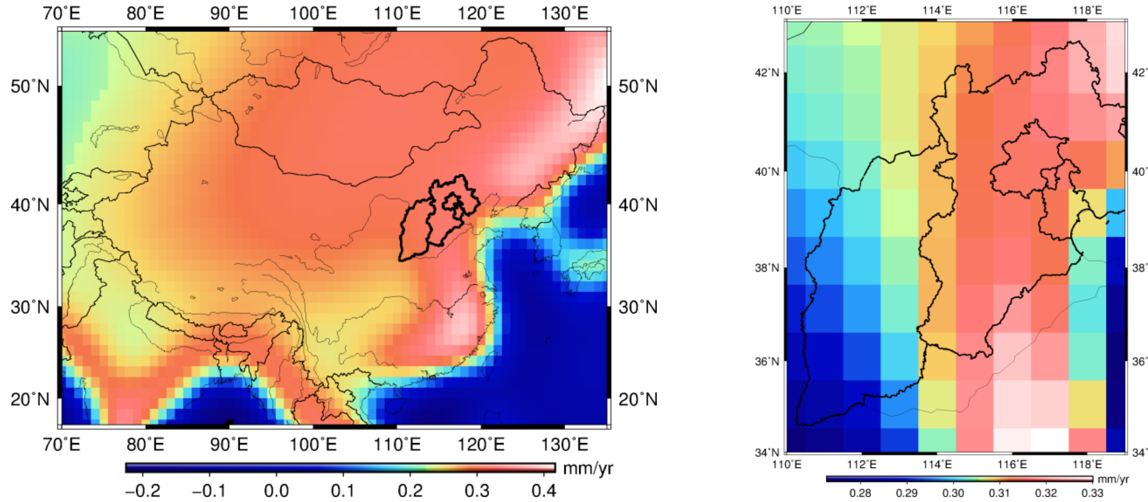

(a) Long-term uplift due to GIA effects in China (b) Long-term uplift due to GIA effects in NCP

Figure S6. The results of vertical crust movement in the NCP from the previous study. (a) The vertical crust movement model between 2007-2013 using GNSS GPS and leveling data, cited from MLR (2015). (b) Vertical motion in north China with high spatial resolution, cited from Zhao et al. (2014)

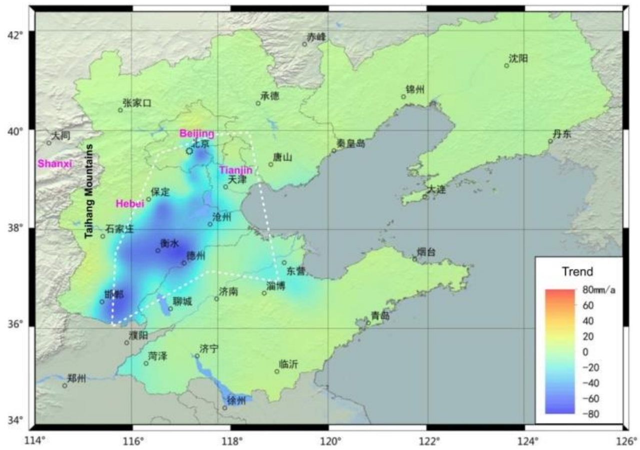

(a)

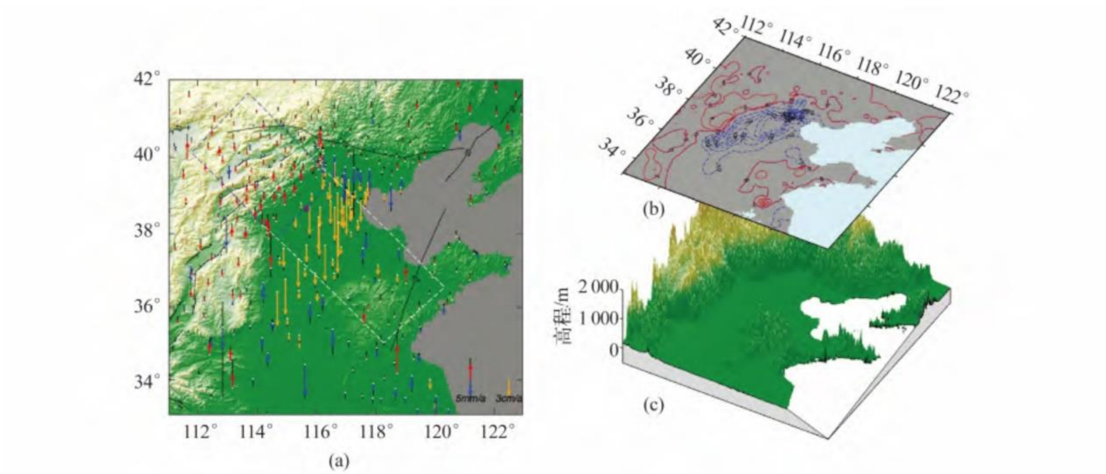

(b)

Table S1. Seasonal amplitudes and phases fit of vertical displacements derived by GRACE and GPS for IGS stations between before and after atmospheric and non-tidal ocean corrected.

Stations	No atmospheric and non-tidal ocean corrected				After atmospheric and non-tidal ocean corrected			
	Annual Amplitude (mm)/ Phase (days)		Semi-annual Amplitude (mm) Phase (days)		Annual Amplitude (mm)/ Phase (days)		Semi-annual Amplitude (mm) Phase (days)	
	GPS	GRACE	GPS	GRACE	GPS	GRACE	GPS	GRACE
BJFS*	3.33/337.56	3.23/311.53	1.56/54.38	0.94/61.83	2.50/40.09	1.35/359.63	1.01/90.09	0.59/71.20
BJSH*	2.75/333.79	3.11/311.81	1.04/74.57	0.86/62.91	3.25/52.75	1.25/1.00	0.68/93.97	0.50/73.76
JIXN*	3.66/314.05	3.24/310.41	1.16/67.54	0.86/63.54	2.46/32.20	1.32/359.72	0.66/81.98	0.53/73.08
TAIN*	4.65/316.75	4.18/308.41	1.71/62.57	1.22/65.95	3.31/16.44	2.07/349.43	1.48/68.35	0.99/74.27
ZHNZ*	4.14/307.37	4.76/312.86	0.75/37.63	1.14/60.31	2.48/28.18	2.24/354.76	0.36/55.63	0.86/73.54

*IGS sites: the observation time between 2003 and 2013.

Table S2. Love numbers from Guo et al. (2004), Han and Wahr (1995).

Degree	Some atmospheric pressure-load Love numbers (Guo et al., 2004)			Some Love numbers from Han and Wahr (1995)			Some Love numbers from ADO1B products
l	h_l	k_l	l_l	h_l	k_l	l_l	k_l
0	–0.13206	0.00000	0.00000	–0.13273	0.00000	0.00000	0.00000
1	–0.28569	0.00000	–0.89642	–0.28796	0.00000	0.10283	0.00000
2	–0.99093	–0.60314	–0.06055	–0.99016	–0.30253	0.02388	–0.30800
3	–1.05012	–0.28787	0.05520	–1.04998	–0.19413	0.06984	–0.19500
4	–1.05281	–0.17494	0.04854	–1.05306	–0.13232	0.05841	–0.13200
5	–1.08577	–0.12889	0.03779	–1.08622	–0.10368	0.04588	–0.10300
6	–1.14331	–0.10696	0.03188	–1.14380	–0.08950	0.03832	–0.08900
7	–1.21204	–0.09478	0.02889	–1.21224	–0.08135	0.03396	–0.08200
8	–1.28335	–0.08646	0.02723	–1.28358	–0.07593	0.03126	–0.07800
10	–1.42263	–0.07595	0.02547	–1.42240	–0.06862	0.02809	–0.06820
18	–1.87337	–0.05618	0.02303	–1.87087	–0.05330	0.02364	–0.05289
32	–2.33483	–0.03979	0.01989	–2.32786	–0.03870	0.01987	–0.03875
56	–2.67593	–0.02527	0.01444	–2.66104	–0.02488	0.01423	–0.02504
100	–2.96478	–0.01443	0.00893	–2.93459	–0.01428	0.00859	–0.01461

Table S3. Correlation between GPS and GRACE derived seasonal variations and WRMS reduction ratio of remove GRACE-derived seasonal deformation from GPS observed detrended height time series (between no corrected and after atmospheric and non-tidal ocean corrected).

Stations	No atmospheric and non-tidal ocean corrected		After atmospheric and non-tidal ocean corrected	
	Correlation (%)	WRMS reduction (%)	Correlation (%)	WRMS reduction (%)
BJFS*	89.83	56.05	73.42	29.37
BJSH*	92.47	58.31	62.83	18.94
JIXN*	99.62	84.75	81.52	36.59
TAIN*	98.73	80.75	87.82	45.97
ZHNZ*	98.68	76.52	77.91	33.23
BJGB#	90.87	53.92	86.44	27.79
BJYQ#	95.63	57.30	89.14	30.38
HAHB#	98.38	77.74	79.84	37.98
HAJY#	89.70	54.28	59.30	21.59
HECC#	98.85	69.01	99.64	45.16
HECD#	85.44	48.68	85.18	25.33
HECX#	90.39	41.49	62.95	19.04
HELQ#	97.48	77.27	78.44	37.80
HELY#	96.81	69.66	86.46	47.63
HETS#	84.89	37.39	18.04	–5.08
HEYY#	99.02	58.98	94.91	35.28
HEZJ#	97.98	59.20	82.74	36.21
NMTK#	96.85	43.08	90.55	25.92
NMZL#	98.56	65.88	84.99	41.86
SDJX#	96.71	73.35	63.49	19.01
SDZB#	86.08	49.36	75.34	30.13
SXCZ#	91.37	58.64	77.93	31.36
SXGX#	83.06	18.79	8.17	–18.67
SXLF#	97.02	74.30	89.12	42.99
SXLQ#	97.96	66.11	91.85	36.22
SXXX#	95.77	68.60	81.01	38.91
TJBD#	91.49	57.02	84.68	32.39
TJBH#	68.23	27.52	61.45	13.38
TJWQ#	81.93	38.52	77.26	21.53

*IGS sites: the observation time between 2003 and 2013.

#CMONOC sites: the observation time between 2010 and 2013.

Table S4. Seasonal amplitudes and phases, trend fit of vertical displacements derived by GRACE, remove GLDAS-derived deformation from GRACE and GIA effects for all GPS stations.

Stations	Lat.	Lon.	Annual Amplitude (mm)		Semi-annual Amplitude (mm)		Trend Rates (mm/yr)		Trend Rates (mm/yr)
			GRACE	GRACE-GLDAS	GRACE	GRACE -GLDAS	GRACE	GRACE -GLDAS	GIA
BJFS[*]	39.6	115.8	1.35	0.66	0.59	0.31	0.53	0.54	0.30
BJSH[*]	40.2	116.2	1.25	0.68	0.50	0.26	0.48	0.49	0.30
JIXN[*]	40	117.5	1.32	0.66	0.53	0.29	0.46	0.50	0.30
TAIN[*]	36.2	117.1	2.07	0.59	0.99	0.29	0.42	0.42	0.31
ZHNZ[*]	34.5	113.1	2.24	0.92	0.86	0.22	0.24	0.17	0.27
BJGB[#]	40.6	117.1	1.25	0.70	0.45	0.25	0.43	0.44	0.30
BJYQ[#]	40.3	115.9	1.23	0.70	0.48	0.26	0.48	0.47	0.30
HAHB[#]	35.6	114.5	2.13	0.74	0.93	0.24	0.32	0.26	0.28
HAJY[#]	35.1	112.4	2.05	0.89	0.85	0.30	0.34	0.32	0.27
HECC[#]	40.8	115.8	1.17	0.76	0.42	0.23	0.44	0.41	0.30
HECD[#]	41	117.9	1.27	0.74	0.42	0.24	0.36	0.38	0.30
HECX[#]	38.4	116.9	1.62	0.66	0.78	0.39	0.54	0.61	0.30
HELQ[#]	38.2	114.3	1.67	0.76	0.79	0.40	0.51	0.51	0.29
HELY[#]	37.3	114.7	1.88	0.73	0.90	0.39	0.47	0.48	0.29
HETS[#]	39.7	118.2	1.39	0.68	0.57	0.31	0.43	0.49	0.29
HEYY[#]	40.1	114.1	1.20	0.72	0.50	0.28	0.49	0.44	0.29
HEZJ[#]	40.8	114.9	1.13	0.77	0.42	0.24	0.44	0.39	0.30
NMTK[#]	40.2	111.2	1.02	0.72	0.47	0.28	0.43	0.35	0.29
NMZL[#]	42.2	115.9	1.15	0.94	0.32	0.22	0.31	0.25	0.30
SDJX[#]	35.4	116.3	2.22	0.62	1.00	0.23	0.35	0.27	0.31
SDZB[#]	36.8	117.9	1.90	0.65	0.93	0.34	0.45	0.48	0.31
SXCZ[#]	36.2	113.1	1.93	0.85	0.88	0.37	0.41	0.38	0.28
SXGX[#]	36.2	111.9	1.81	0.93	0.83	0.44	0.47	0.44	0.27
SXLF[#]	36	111.3	1.79	0.97	0.81	0.45	0.49	0.46	0.27
SXLQ[#]	39.3	114	1.38	0.72	0.62	0.33	0.51	0.48	0.29
SXXX[#]	35.1	111.2	1.98	0.98	0.82	0.37	0.40	0.40	0.27
TJBD[#]	39.6	117.3	1.38	0.65	0.59	0.31	0.49	0.55	0.30
TJBH[#]	39	117.6	1.49	0.67	0.68	0.35	0.51	0.58	0.29
TJWQ[#]	39.3	117.1	1.43	0.65	0.64	0.34	0.52	0.58	0.30

[*]IGS sites: the observation time between 2003 and 2013.

[#]CMONOC sites: the observation time between 2010 and 2013.